Nano Energy 37 (2017) 108–117

Contents lists available at ScienceDirect

Nano Energy

journal homepage: www.elsevier.com/locate/nanoen

Full paper

Graphene nanowires anchored to 3D graphene foam via self-assembly for high performance Li and Na ion storage

Xiaoxu Liu[a,b,1], Dongliang Chao[d,1], Dapeng Su[a], Shikun Liu[a], Liang Chen[a], Caixia Chi[a], Jianyi Lin[d], Ze Xiang Shen[d], Jiupeng Zhao[a,*], Liqiang Mai[c,*], Yao Li[a,*,1]

[a] School of Chemistry and Chemical Engineering, and ‖Center for Composite Materials and Structure, Harbin Institute of Technology, Harbin 150001, China
[b] Key Laboratory for Photonic and Electric Bandgap Materials; Institute of Advanced Composite Material Technology, Heilongjiang University of Science and Technology, Harbin 150022, China
[c] State Key Laboratory of Advanced Technology for Materials Synthesis and Processing, Wuhan University of Technology, Wuhan 430070, China
[d] Division of Physics and Applied Physics, Nanyang Technological University, 637371, Singapore

ARTICLE INFO

Keywords:
Graphene nanowires
3D all-graphene electrode
High performance
Li and Na ion batteries

ABSTRACT

Graphene has been extensively investigated as anode material for Li and Na ion batteries due to its excellent physical and chemical performance. Herein, we report a new member of 'graphene family', a reduced graphene nanowire on three-dimensional graphene foam (3DGNW). The novel graphene nanowires were synthesized via a template strategy involving reduction and assembly process of nanosized graphene oxides (nGO), pyrolysis of polystyrene spheres (PS) template and catalytic reaction between GO and PS decomposition products. When evaluated as anodes material for Li and Na ion batteries, the 3DGNW exhibits relatively low discharge-voltage plateau, excellent reversible capacity, rate capability, and durable tolerance. For anode of Na ion batteries, a reversible capacity of more than 301 mAh g^{-1} without capacity fading after 1000 cycles at rate of 1 C were achieved. Even at rate of 20 C, a high reversible capacity of 200 mAh g^{-1} can be retained. The superior electrochemical performance is ascribed to hierarchical multidimensional graphene architecture, high graphene crystallinity, expansile graphene interlayer distance, and extensively lateral exposed edges/pores, which can promote the electron and ion transport. The realization of assembling reduced graphene sheets to graphene nanowire offers new opportunities for energy storage application of graphene based assembly in future.

1. Introduction

In the pursuit of high energy- and power-density rechargeable batteries for energy storage systems, graphene, a single atomic layer of carbon arranged in a two-dimensional honeycomb lattice, has become one of the hottest materials due to its excellent characteristics including high chemical stability, electrical conductivity, and surface area [1–9]. Planar single layer graphene was initially produced for fundamental researches in limited quantities by the micromechanical cleavage method [10]. Chemical vapor deposition method was later established to produce high-quality graphene in the form of large area, which was a well-established technique for the synthesis of high quality graphene [11]. However, high temperature and metal catalysts required in the method are cost ineffective. Keith R. Paton et al. have shown that high-shear mixing of graphite in suitable stabilizing liquids results in large-scale exfoliation to give dispersions of graphene nanosheets by liquid-media exfoliation method. However, this process still leaves a considerable amount of unexfoliated graphite [12]. Beyond the aforementioned methods, modified Hummers method has been widely employed by strong oxidation of pristine graphite, followed by chemical, thermal or electrochemical reduced processes [13–15]. Despite the obtained reduced graphene oxide (rGO) material having both intrinsic defects and extrinsic defects, the rGO using as building block was easily constructed 2D and 3D graphene macrostructures including graphene film, graphene hydrogel and graphene aerogel [16]. To date, although a great number of reports highlighted the rGO advantages (high capacity, capability, and durable tolerance) for application of lithium-ion batteries (LIBs) and sodium ion batteries (SIBs) [17,18], their limitations, including a high discharge-voltage plateau [19], low initial coulombic efficiency [20], and low volume energy density, cannot be neglected. While planar graphene growth has received significant attention, construction of 1D graphene nanostructures with micrometers in length is a particularly attractive solution to the above-mentioned limitations owing to their unique physical and chemical

* Corresponding authors.
E-mail addresses: jpzhao@hit.edu.cn (J. Zhao), mlq518@whut.edu.cn (L. Mai), yaoli@hit.edu.cn (Y. Li).
[1] These authors contributed equally to this work.

http://dx.doi.org/10.1016/j.nanoen.2017.04.051
Received 21 February 2017; Received in revised form 14 April 2017; Accepted 24 April 2017
Available online 27 April 2017

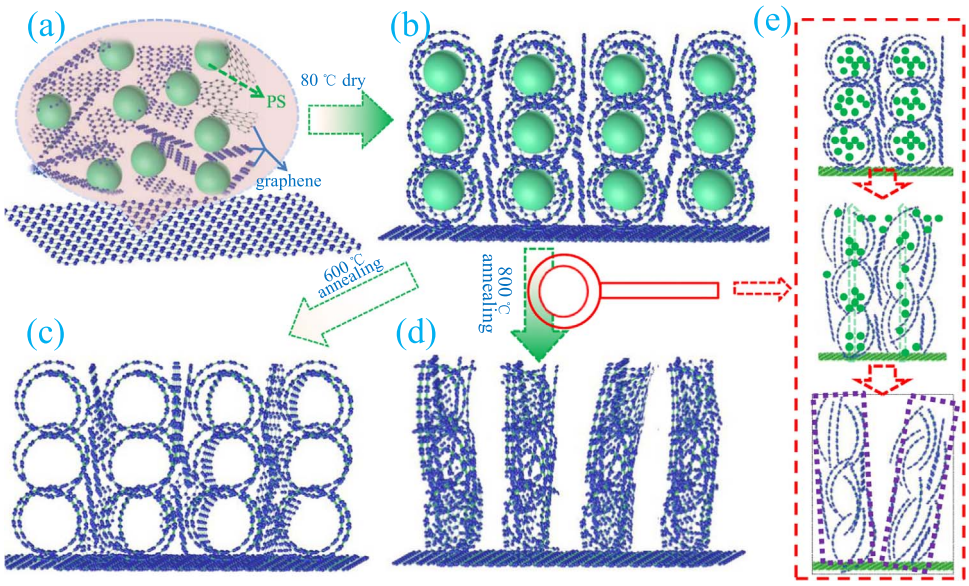

Fig. 1. Schematics for the fabrication of graphene nanowires. a) An aqueous solution with nGO and PS spheres dropwise added to surface of NF with mGO. b) nGO and PS spheres coated on the surface of mGO after evaporation of water. c) A solid-state pyrolysis process at 600 °C for the removal of PS spheres template. d) A solid-state pyrolysis process at 800 °C for the removal of PS spheres template and assembly of nGO sheets. e) Schematics of the formation process of the graphene nanowires.

properties. Nevertheless, approaches to 1D graphene have been relatively less explored. To date, graphene scrolls (GS) have been reported through rolling mechanism of a graphene sheet. For example, L. Mai el al. had designed nanowire templated semihollow bicontinuous graphene scroll architecture by "oriented assembly" and "self-scroll" strategy. Meanwhile, lithium batteries based on V_3O_7 nanowire templated graphene scrolls exhibited an excellent performance with specific capacity of 321 mAh g^{-1} at 100 mA g^{-1} and capacity retention of 87.3% after 400 cycles at 2000 mA g^{-1} [21]. Young-Eun Shin et al. introduced an ice-templated self-assembly approach for the integration of two-dimensional large graphene nanosheets into hierarchically porous GS, showing promising electrocatalytic activity for the oxygen reduction reaction [22]. C. Gao et al. developed a well-controlled freeze-dry method to scroll 2D large size graphene sheets to 1D GS in high efficiency up to the yield of 92% [23]. Long GS architecture may provide novel opportunities for enhancing electron transport, however, the lithium or sodium ion diffusion coefficient in axial direction of GS is much larger than that of vertical direction. If small size graphene can be assembly into graphene nanowires, and the exposed graphene layers and pores can be perpendicular to the axial direction of the nanowires, which would be beneficial to both ionic and electronic transport. Such structure with self-assembled nanosized graphene into long graphene nanowires has not yet been achieved in previous reports.

Here for the first time we achieved a novel carbonaceous anode, the graphene nanowires anchored to three-dimensional graphene foam (3DGNW), through a simple template strategy involving self-assembly process of graphene sheets, removal of polystyrene spheres (PS) template and thermal activation. The 3DGNW electrode was achieved by assembly of graphene with different size where the exposed small size graphene is partially perpendicular to the axial direction of the graphene nanowires, and graphene nanowires is also partially perpendicular to large size graphene layer substrate. The prepared all-graphene electrode exhibits relatively low discharge-voltage plateau, good reversible specific capacity, excellent rate capability, and durable cycling stability for both Li and Na ion batteries because of their hierarchical three-dimensional carbon architecture, high graphene crystallinity and expansible graphene interlayer distance. This unique micro-/nanostructures are beneficial to achieving high energy and power densities: (i) the graphene nanowire structure on graphene foam constitutes an effective multi-dimensional conductive network for bi-continuous fast electron transport. (ii) The micro-sized graphene nanowires in length with high crystallinity, axial graphene lattice arrangement, lateral edges/pores, and expansible graphene interlayer distance enable fast charge transfer redox reaction and convenient ions insertion/extraction. (iii) This light-weight freestanding all-carbon 3DGNW affords improved energy density of the whole electrode due to elimination of the metal current collector, additional binder and carbon additives. As expected, the 3DGNW anode delivered a high reversible lithium storage capacity of 545 mAh g^{-1} at a current density of 0.1 C (1 C=372 mA g^{-1}) with a high initial coulombic efficiency of 74%, which is much higher than other pure rGO anodes in literatures. Moreover, a sodium storage capacity of 497 mAh g^{-1} was obtained when it is used as electrode for SIB. A specific capacity as high as 201 mAh g^{-1} can be achieved at 20 C, which is significantly higher than conventional carbonaceous SIB anodes [24–27]. Moreover, no obvious capacity fading is observed after more than 1000 cycles of continuous charge/discharge.

2. Experimental

2.1. Preparation of the graphene oxide (GO)

Briefly, 3*g* of natural graphite powder was added to concentrated sulfuric acid (400 mL) at 0 °C. Then, 6*g* of $KMnO_4$ was added slowly until dissolved. The reaction was kept at 35 °C for 2 h. Next, the mixture was added to 400 mL deionized (DI) water and heated to 90 °C for 1 h. (Note: This solution is very corrosive. It reacts violently with organic material, and it must be treated with extreme caution.) Then the solution was centrifugated at 6000 rpm/min. The sediment was decanted, and the remaining solution was further dialyzed in a dialysis bag (retained molecular weight: 3500 Da) for 3 days. Finally, nano-sized GO sheets (nGO) suspension was obtained (the average area of nGO is 2500-10^4 nm^2 , as shown in Fig. S1). The sediment was washed with a total of 500 mL of 5% HCl solution for 3 times, and then washed with DI water for 10 times to get the micro-sized GO (mGO) suspension (the average size of mGO is around 200 μm, as shown in Fig. S2).

2.2. Preparation of the graphene nanowires anchord to 3D graphene foam

The experimental procedure for the preparation of the 3DGNW is

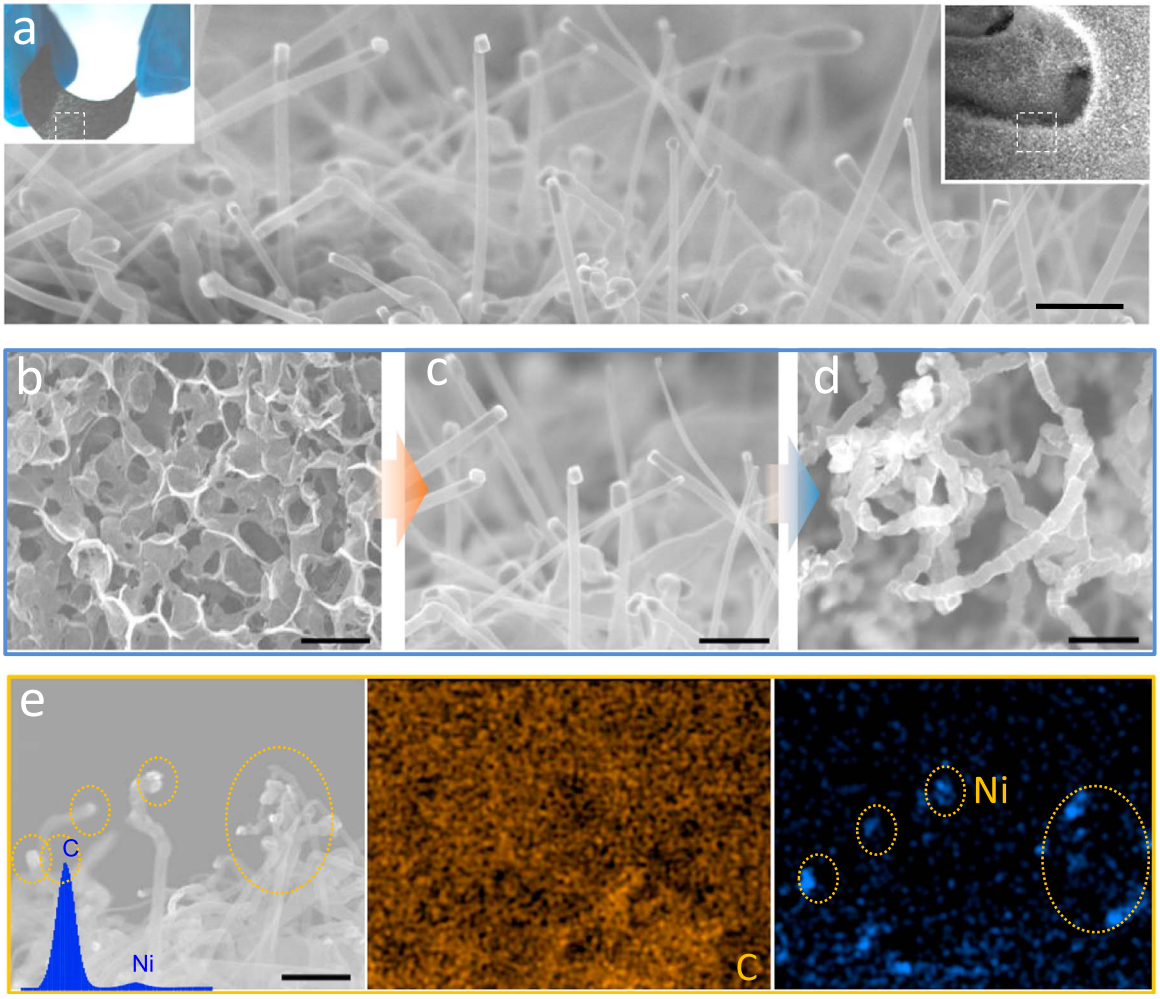

Fig. 2. SEM images of 3DGNW under different reaction conditions. a) SEM image of 3DGNW obtained at annealing temperature of 800 °C. Left inset: Digital photo of 3DGNW that is bent by a small force to show its flexibility. Right inset: Low magnification SEM image of 3DGNW. b) SEM image of 3DPG foam. c–d) SEM images of 3DGNW obtained from different suspensions with concentrations of 10 and 20 mg mL^{-1}. e) EDS element mapping of C and Ni of the 3DGNW. Scale bar: 500 nm.

schematically shown in Fig. 1. Typically, nickel foam (NF) sheets (4×1.5×0.1 cm, mass per unit area 45 mg cm^{-2}) were immersed in the mGO suspension (0.5 mg mL^{-1}), which was followed by sonication for 10 min to ensure the successful filling of the mGO suspension into the micropores of the NF. Subsequently, the NF sheets were allowed to dry at 80 °C overnight. After cooled to room temperature, an ultrathin layer of mGO was uniformly coated on the NF. Then, 3 mL polystyrene (PS) spheres suspension (average particle size is 500 nm and the concentration is 5 wt%, as shown in Fig. S3) which were obtained using emulsion-free emulsion polymerization technology [28] was added in 15 mL of nGO (2 mg mL^{-1}) suspension under magnetic stirring to form a PS and nGO mixed suspension. The concentration of nGO and PS of the mixed suspension is calculated to be 10 mg mL^{-1} and the mass ratio of nGO and PS is 1:5. The GO coated NF sheets were immersed into the mixed suspension and then dried at 80 °C to remove water. The dried samples were calcinated in Ar at 200 °C for 1 h and then 800 °C for 2 h. Finally, free-standing 3DGNW was obtained via etching of NF in a mixture solution of 1 M $FeCl_3$ and 0.5 M HCl for 10 h at room temperature.

2.3. Electrochemical measurements

The electrochemical properties of the samples were evaluated using CR 2032 coin cells. The coin cells were assembled in a glove box filled with high-purity argon, where the as-fabricated 3DGNW anodes without binder and conductive additives were used as the working electrode. For lithium ion battery fabrication, the metallic lithium foil was used as the counter-electrode, 1 M $LiPF_6$ in ethylene carbonate (EC)-dimethyl carbonate (DMC) (1:1 in volume) was used as the electrolyte, and a polypropylene (PP) film (Cellgard 2400) was used as the separator. For sodium ion battery fabrication, metallic Na foil was used as the counter/reference electrode, glass fiber (Whatman) was used as the separator, and 1 M $NaClO_4$ in ethylene carbonate (EC)-diethyl carbonate (DEC) (1:1 in volume) was used as the electrolyte. The discharge-charge performance of the batteries was tested using battery analyzer (Neware CT-3008) with the voltage cut-off between 0 and 3.0 V vs. Na/Na^+. The electrochemical impedance spectroscopy (EIS) and cyclic voltammetry (CV) measurements were performed using a CHI660E electrochemical workstation. EIS was recorded with a frequency ranging from 100 kHz to 10 mHz and a AC signal of 5 mV in amplitude as the perturbation. The voltage range of the CV measurements was 0–3.0 V and the scanning rate was 0.5 mV/s. All the tests were performed at room temperature.

3. Results and discussion

The overall preparation procedure of 3DGNW is schematically shown in Fig. 1. A 3D interconnected graphene oxide (GO) network on Ni foam was formed via micro-sized GO (mGO) coating. Then, an aqueous suspension of nano-sized GO (nGO) and PS spheres was repeatedly dropwise added to the coated mGO Ni foam (Fig. 1a). A graphene nanowire (GNW) was obtained from self-assembly of nGO

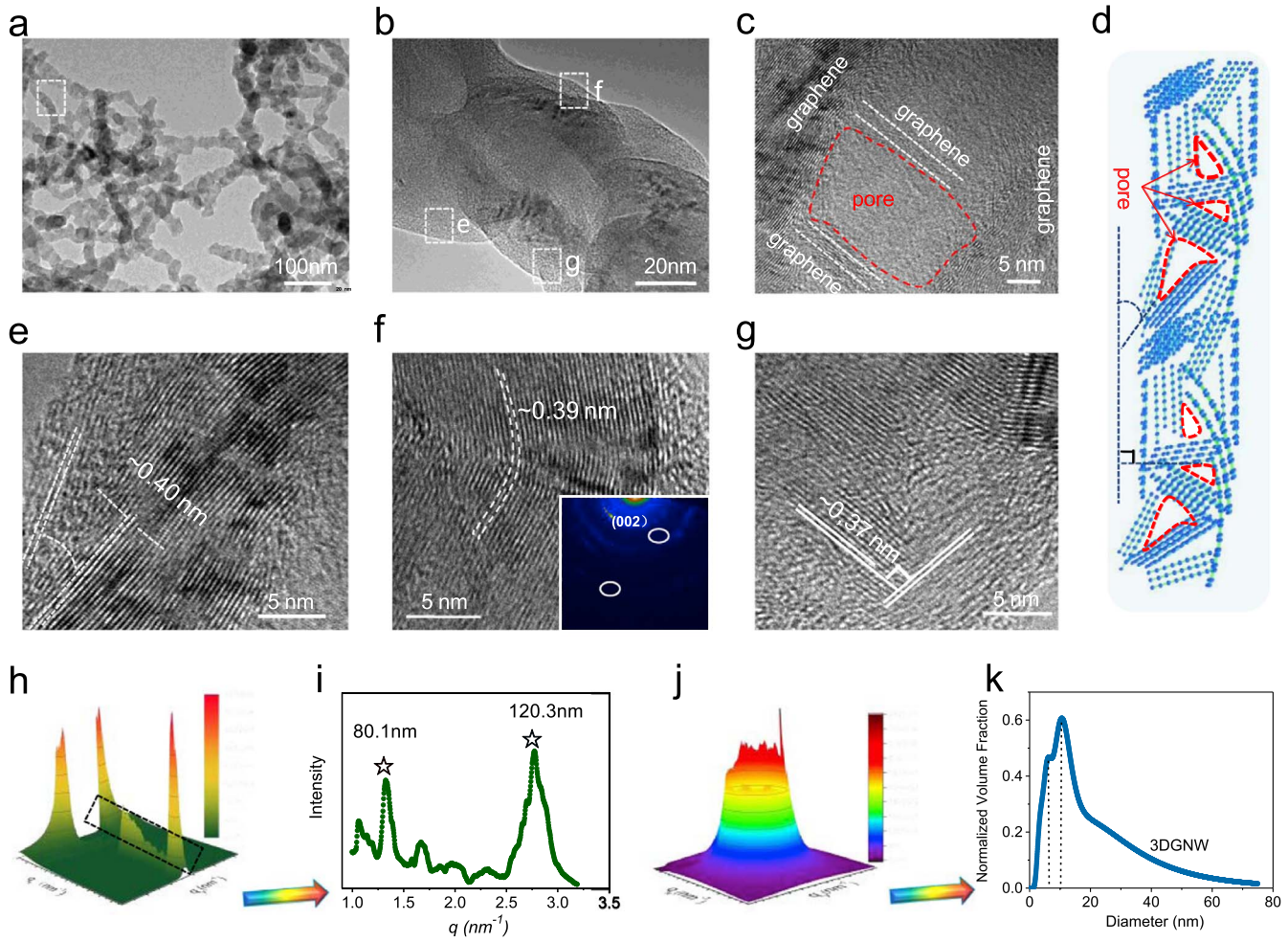

Fig. 3. Structure characterization of 3DGNW. a-c) TEM and HRTEM images of 3DGNW. d) A model of GNWs from assembly of graphene sheets. e-g) HRTEM images taken from the square regions in Fig. 3b. Inset in Fig. 3f: SAED pattern. h, i) The GISAXS patterns and scattering curve of the 3DGNW. j, k) The SAXS patterns and pore size distribution of the 3DGNW.

after solid-state thermal reduction process at 800 °C (Fig. 1d). After removal of NF by HCl, a flexible freestanding 3DGNW is produced. Fig. 2a and S4 are the SEM images of 3DGNW. The graphene foam is covered with entangled nanowires slightly vertically oriented. The typical length of the nanowires is longer than 1 μm with an average diameter of 80–120 nm. The digital image in the left inset of Fig. 2a shows a free-standing 3DGNW with black color, indicating good flexibility. The area density of 3DGNW is about 0.5–0.8 mg cm^{-2}, which demonstrates the light-weight of the foam (Table S1). The multi-dimensional structure of 3DGNW with interconnected 3D micro-size pores and the long graphene nanowires can facilitate the ion diffusion when it is used as an electrode material.

In the experiment, the annealing temperature, the concentration of nGO and PS spheres, substrate and the size of the graphene sheets play crucial rules in the formation of nanowires. In order to further understand the formation mechanism of the GNW, control experiments have been done. When the annealing temperature is 600 °C, instead of formation of GNW, 3D interconnected porous graphene frameworks (3DPG) were found (Figs. 1c,2b and S5). The formation of GNW is also dependent on the concentration of nGO and PS spheres. When the concentration is increased to 20 mg mL^{-1} (the mass ratio of nGO and PS is fixed at 1:5), the resultant GNWs become more disordered and tangled (Fig. 2d). The quality of GNWs was decreased with the decreasing concentration. When it is 5 mg mL^{-1}, only a few GNWs could be formed (Fig. S6). In the absence of PS or GO, or with their concentration < 2.5 mg mL^{-1} (Figs. S7-9) or replacing nGO with mGO, the GNWs could not be formed. We have also using Cu foam to do the control experiment to confirm that NF is essential in the formation of GNWs. Three-dimensional porous structure instead of GNWs is formed on the Cu foam under identical conditions (Fig. S10). Based on the above experimental results, we propose a possible GNWs formation mechanism of PS pyrolysis, disintegration of the 3D porous graphene skeleton, and rearrangement of nGO sheets. First, PS spheres were wrapped by nGO sheets, and act as the template. It is known that the decomposition of PS starts at ~400 °C, and the main products are styrene trimer, dimer and monomer [29]. During the annealing process at 800 °C, the multi-monomers completely decompose to low molecular weight carbon fragment products or radical products in 3D porous graphene skeleton (see Fig. 1e). Then, these low molecular weight carbon fragment products may react with GO sheets [30], serving as a reductant and glue to reduce GO. Meanwhile, Ni foam serves as the source of catalyst [31], which can promote reactions between graphene sheets and low molecular weight carbon fragment products (tiny nickel particles were found at the top of GNW shown in Fig. 2e). During the reaction, a large of amount of gases are violently released, leading to disintegration of the 3D porous graphene skeleton (see Fig. 1e). Last, the reaction proceeds fast between graphene oxide with the increase of reaction time, leading to spontaneous and self-driven sliding [32] and coalescence of nanosized graphene sheets. Due to the confinement effect of PS template, graphene sheets were assembled along disintegrated 3D graphene skeleton, leading to the formation of the GNWs.

The structural properties of 3DGNW were further studied by TEM at different magnifications. The low magnification TEM images clearly show that the diameter of the GNWs is about 80–100 nm (Fig. 3a, b),

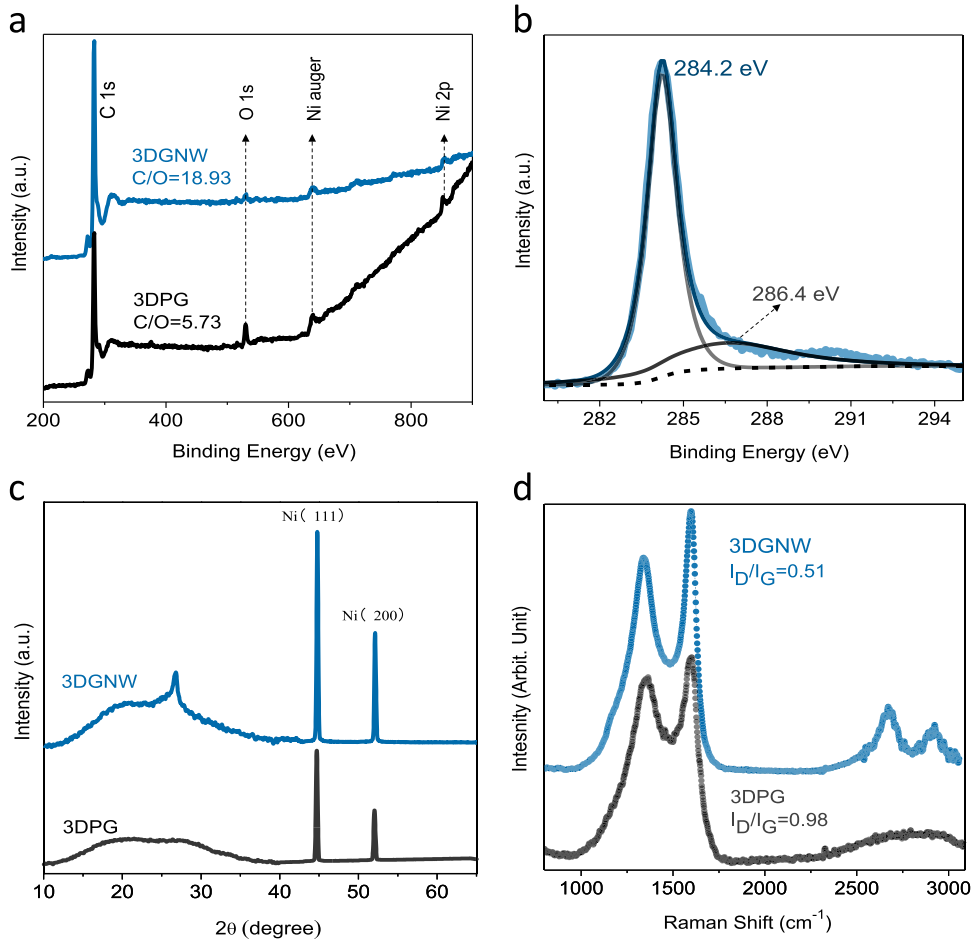

Fig. 4. (a)XPS spectra of the 3DGNW and 3DPG samples; (b) XPS C1s spectra of the 3DGNW and 3DPG samples; (c) XRD patterns and (d) Raman spectra of the 3DGNW and 3DPG samples.

and the corresponding high-magnification TEM images (Fig. 3c) shows that the GNW consists of graphene crystallines with different sizes and nano-pores (see a model in Fig. 3d), which is benefited for buffer the volume expansion, using as electrode materials of lithium ion battery or sodium ion battery. Interestingly, the GNWs display well-defined graphene layers with long-range order stacking parallel to each other, as shown in HRTEM images taken from the square regions in Fig. 3b (Fig. 3e-g). The GNWs show higher crystallized graphitic structure than that of the 3DPG foam, which was obtained at annealing temperature of 600 °C (Figs. S11,12) and previous reports RGO [33–35]. In addition, the progressive change in interlayer distance is apparent. The average interlayer spacing is measured to be 0.40 nm in Fig. 3e, 0.39 nm in Fig. 3f and 0.37 nm in Fig. 3g, which is larger than that of graphite (0.34 nm). It is obvious that the distances between GNW layers expand due to the residual oxygen-containing groups after thermal treatments. Furthermore, the selective area electronic diffraction (SAED) pattern in HRTEM image (inset in Fig. 3f) shows the (002) graphitic structure. With the development of synchrotron X-ray technology, small angle X-ray scattering (SAXS) technique is widely used as an effective measurement to probe the nanoscale structures in materials. For further determining the structure of the 3DGNW, the synchrotron grazing-incidence small-angle x-ray scattering (GISAXS) and vertical-incidence SAXS were used. The 3DGNW exhibits an anisotropic three-dimensional GISAXS pattern (Fig. 3h), which further proves the existence of oriented wirelike structure, and the average diameter of GNWs is about 80.1–121.3 nm, calculated according to GISAXS theory [36–38] (see Fig. 3h, i). However, the scattering point characterized anisotropic microstructure is not founded in GISAXS pattern of 3DPG foam (see Fig. S13). Fig. 3j shows the 3D SAXS patterns of 3DGNW, which confirm that the GNWs are uniformly distributed in a direction parallel to the sample surface. The porous size distribution of the 3DGNW is shown in Fig. 3k and the relative pore size distribution derived from SAXS method shows the peaks at 8 and 10 nm, suggesting a highly porous feature of the 3DGNW [39]. The appearance of the ~10 nm pores derives from the interstices between graphene sheets in Fig. 3c. The structural characteristics of the 3DGNW electrode, including hierarchical multidimensional carbon architecture, high graphene crystallinity, expansile graphene interlayer distance, and nanoporous feature are vital for superior Li/Na^+ storage performance, especially for high-rate capability and high power/energy density.

The detailed surface chemistry of the 3DGNW and 3DPG samples was characterized by XPS measurements and the results are shown in Fig. 4a. The survey scan spectra from XPS analysis of the 3DGNW and 3DPG foam show the presence of the principal C1s, O1s, and Ni1s core levels, with no evidence of impurities. The oxygen content of the 3DGNW is obviously lower than that of 3DPG sample, while the calculated C/O ratio of the 3DGNW (18.9) is much higher than 3DPG sample (5.7) and those of previously reported RGO materials [14]. It could also indicates that the formation of 3DGNW is a result of the reduction of GO by the small molecular fragments derived from high temperature PS pyrolysis. The C1s core level peak can be resolved into two components centered at 284.2 and 286.4 eV, suggesting sp^2 C-sp^2 C and C–O (hydroxyl and epoxy) bonds, respectively (Fig. 4b). And the XPS spectra of O1s peak can be resolved as 531.6 and 533.7 eV, corresponding to the O–C=O and C=O bond, respectively (see Fig. S14). These results suggest the existence of carbonyl and carboxylate groups in 3DGNW. X-ray diffraction (XRD) is an effective technique for

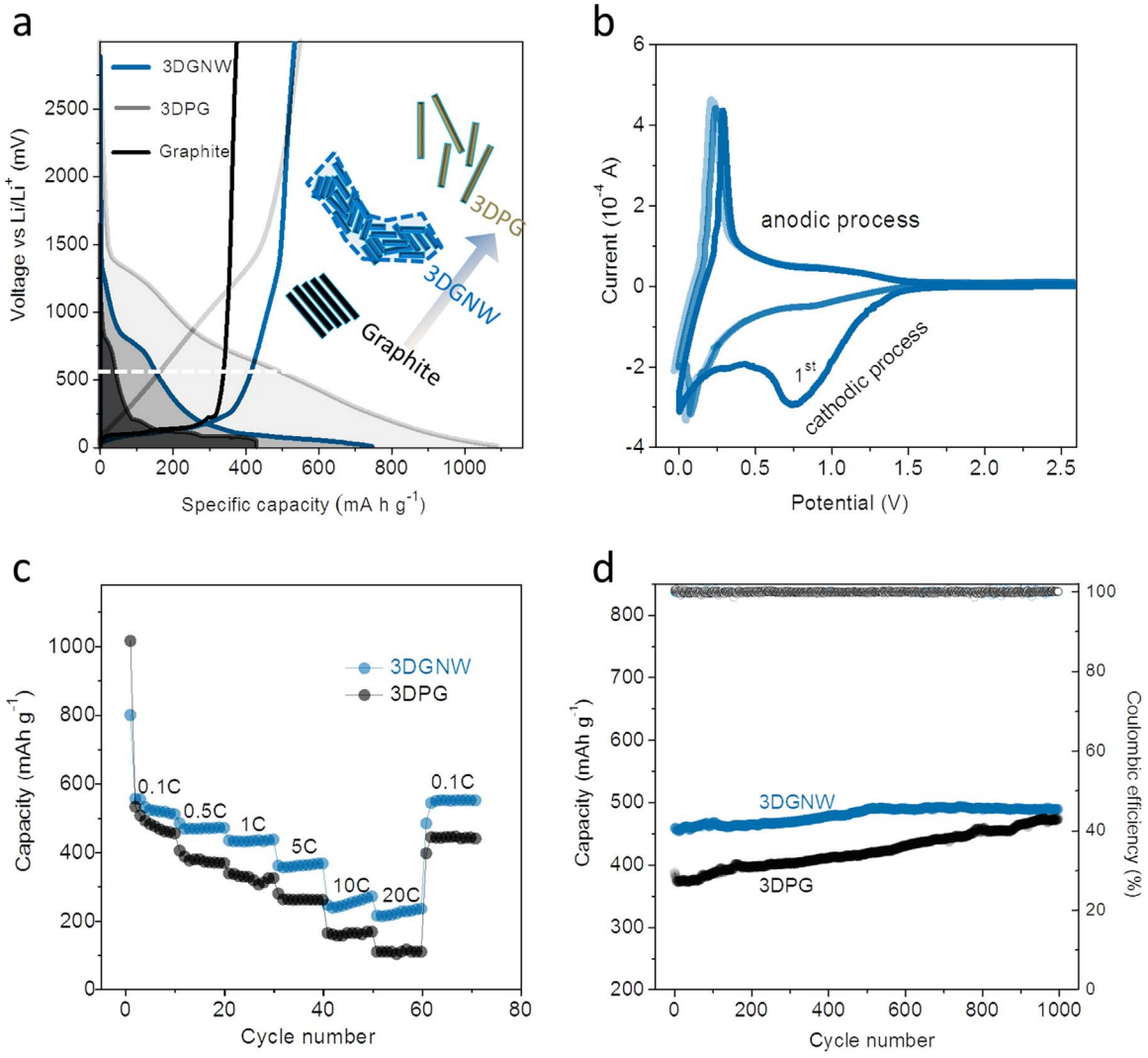

Fig. 5. Quantitative analysis of the lithium storage behavior for 3DGNW. (a) Charge and discharge curves of 3DGNW, 3DPG and graphite at 0.1 C. b) CV curves of the 3DGNW electrode. (b) Rate capability of 3DGNW and 3DPG at various C rates of 0.1, 1, 3, 5, 10 and 20 C. (d) Capacity retention of the 3DGNW and 3DPG electrodes at 1 C.

probing the amount and orientation of graphitic carbon sheets. XRD pattern of the 3DGNW sample shows a sharp (002) peak at ~26° compared to 3DPG sample, suggesting higher crystalline graphitic structure (Fig. 4c). The asymmetric and broad peak at 20.4° is consistent with the increased interlayer spacing due to the residual of oxygenous groups between layers. Two very sharp peaks around 44° and 52° are assigned to peaks from trace amounts residue Ni (111) and (200), respectively. The XRD results are in good agreement with the HRTEM images. Raman spectra of 3DGNW and 3DPG (Fig. 4d) show two obvious intense bands for both samples, namely, G peaks at ca. 1590 cm^{-1} and D peak at ca. 1354 cm^{-1}. The D peaks indicate the defective nature of the obtained 3DGNW, which may originate from the distorted hexagonal sp^2 carbon networks. The intensity ratio between D and G bands (I_D/I_G) is normally used to evaluate the crystalline quality of defected graphene or graphite [40–42]. The I_D/I_G is 0.98 for the 3DPG and 0.51 for the 3DGNW sample, which may suggest better graphitization of 3DGNW. Compared with 3DPG, the 3DGNW exhibits second order 2D and D+G peaks at 2674, and 2897 cm^{-1}, which are characteristic of rGO [43,44].

To further evaluate the 3DGNWs for real device application, the electrochemical performance of the 3DGNW in LIBs was investigated. The voltage plateaus for the first discharge/charge curves of 3DGNW, 3DPG and commercial graphite are shown in Fig. 5a. The plateau of 3DGNW lies between 3DPG and commercial graphite, because the crystallinity and graphene interlayer distance of 3DGNW lies between 3DPG and commercial graphite, which was confirmed by results of TEM and XRD. The first discharge and charge capacities of the 3DGNW anode are 734.7 and 545.6 mAh g^{-1} at 0.1 C rate (1 C=372 mA g^{-1}), respectively, with an initial coulombic efficiency as high as 74.5%. The voltage plateau between 0.75 and 0.80 V might be attributed to the irreversible reaction of the electrode to form the SEI layer on the surface of the electrode. This is also confirmed by representative CV curve of the 3DGNW anode (see Fig. 5b), where the remarkable cathodic peak around 0.7 V disappears in the subsequent cycles. The major discharge capacities of the 3DGNW anode below 0.2, 0.5 and 1 V voltage plateau are more than 40%, 79% and 90% of total discharge capacity (0.01–3 V), respectively. Obviously, such voltage plateau is lower than that of the 3DPG and previous reported rGO anodes (see Fig. S15), which is benefit for improving the power density of the full cell in potential industrial applications. On the other hand, compared with commercial graphite anode, slightly higher discharge plateau is advantageous for suppressing growth of lithium branched crystal for 3DGNW anode during charge and discharge process, which is the safety insurance of the batteries [45]. Besides, the Li storage capacity of 3DGNW anode is much higher than the commercial graphite anode, therefore 3DGNW electrode is a new carbonaceous anode for lithium-ion battery combined the advantages of both graphene and graphite on the electrochemical properties.

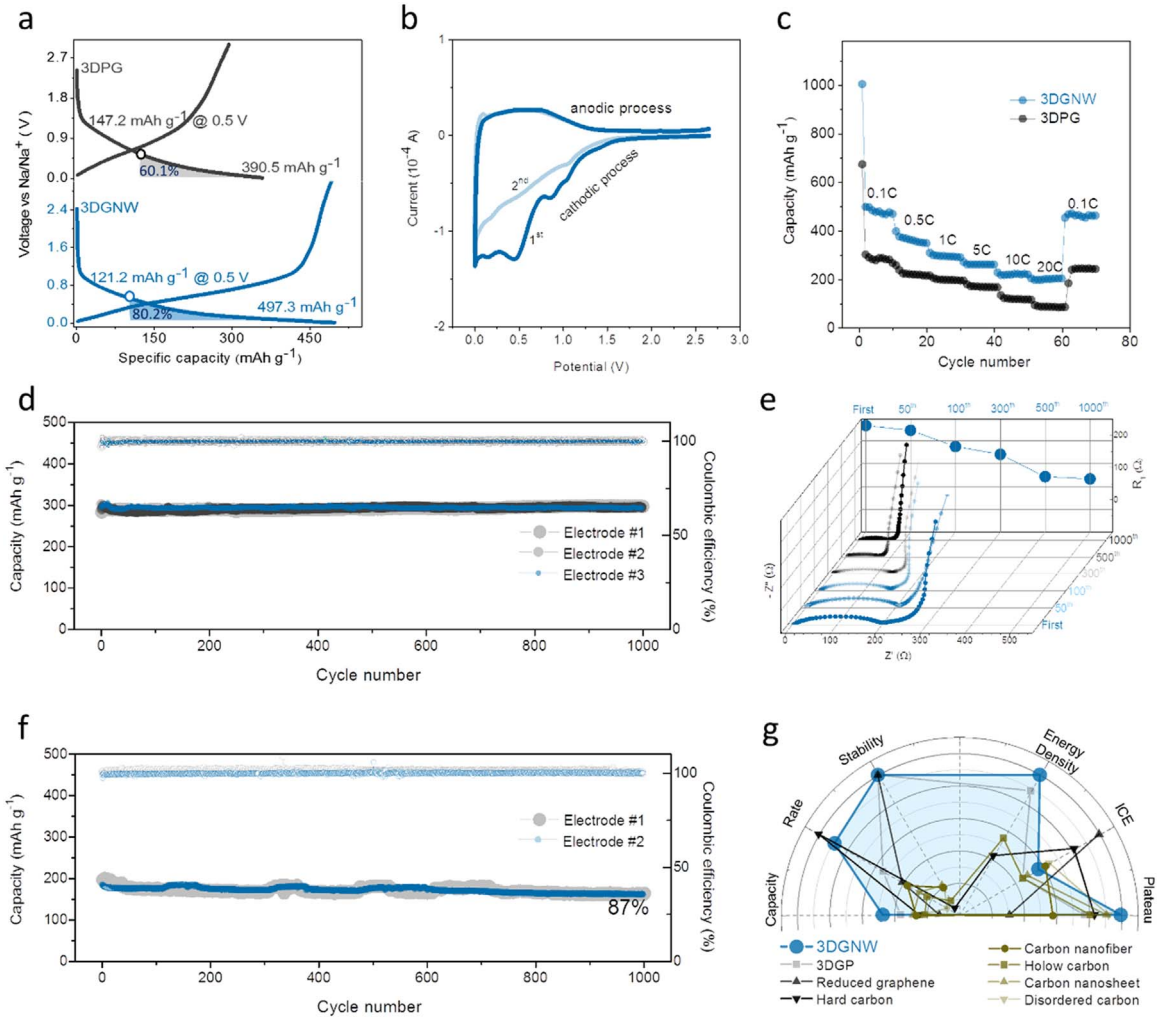

Fig. 6. Electrochemical characterization for SIBs. (a) Charge–discharge curves of 3DPG and 3DGNW for the second cycles at 0.1 C (1 C=372 mA g^{-1}). (b) CV curves of the 3DGNW anode at a scan rate of 0.1 mV/s. (c) Rate performance of the 3DGNW and 3DPG electrodes. (d) Cycling performance of three different 3DGNW electrodes at 1 C for 1000 cycles. (e) AC impedance plots at different cycles of the 3DGNW electrode. The resistance is simulated using the same equivalent circuit R1(Q(R2ZW)C. (f) Cycling performance of three different 3DPG electrodes at 1 C for 1000 cycles. (g) Comparison of 3DGNW electrode and reported pure carbonaceous anode (with normalized capacity, rate, stability, volume energy density and IEC etc.). The area with color indicates the integrated electrochemical storage Na performance.

Fig. 5c further compares the rate performance of the 3DGNW and 3DGP anodes. The 3DGNW anode can deliver a reversible specific capacity of 545.6, 465.4, 446.9, 331.0, 224.7, 201.1 mAh g^{-1} at 0.1, 0.5, 1, 5, 10, and 20 C rates, respectively. However, the 3DPG anode delivers a lower reversible specific capacity of 548.9, 379.4, 327.1, 260.1, 157.5, 101.7 mAh g^{-1} at the same C rates. When the C rate increases 200 times from 0.1 to 20 C, the 3DGNW anode shows high capacity retention ratio of 41%. The better rate performance of 3DGNW anode should be resulted from the expansile graphene interlayer distance and hierarchical microstructure, which promote the fast transport and intercalation kinetics of Li ions. The cycling performances of 3DGNW and 3DPG anodes are given in Fig. 5d. For the 3DGNW anode, the reversible specific capacity increases obviously at the first 400 cycles and maintains a stable reversible specific capacity of ~467 mAh g^{-1} in the following cycles. While the 3DPG anode shows an increasing capacity during 1000 cycles. The increase in the discharge capacities of the 3DGNW and 3DPG after cycles is attributed to the formation of a gel-like reversible polymer film on the surface of graphene layers [46]. Compared to other reported graphene anodes, the 3DGNW anode exhibits excellent Li storage performances [47–50], as summarized in Table S2. Meanwhile, the trace amounts Ni residue in 3DGNW anode shows no negative influence on the lithium storages performance (see Fig. S16).

We also examined the sodium storage performance based on the 3DGNW electrode, and the results are shown in Fig. 6, S17. The charge and discharge capacity of the 3DGNW electrode for the first cycle are 497 and 1003 mA h g^{-1} at 0.1 C, respectively, with an initial coulombic efficiency (ICE) of 49.5%. This value is comparable to the reported results [18,51–55]. It is noted that the discharge profile in Fig. 6a shows a low discharge plateau for the 3DGNW electrode. More than 80% capacity of 3DGNW anode is supplied below 0.5 V, which is much higher than that of the 3DPG anode and previous research on carbonaceous anodes (see Fig. 6g and Table S3). The CV curves of 3DGNW in Fig. 6b exhibit a small broaden peak at 0.4–0.5 V, which is in accordance to the SEI formation [53]. Most carbonaceous anodes used for LIB electrodes may not work well for SIBs because of a sluggish electrochemical kinetics with Na ions [56]. In this work, the judiciously designed 3DGNW electrode structure allows Na^+ uptakes at really high current densities ranging from 0.1 to 20 C. When cycled at high rates, that is, 0.1, 0.5, 1, 5, 10, and 20 C, it can achieve a remarkably stable and high capacity of 497, 361, 296, 256, 224, and 203 mAh g^{-1}, respectively (Fig. 6c). Besides, compared with individual graphene nanowires, the rate performance of 3DGNW is enhanced by pure graphene foam (see Fig. S18). The result is in sharp contrast to those reported carbonaceous anodes, for example, reduced graphene [18,51], graphite [57,58], hard carbon [59,60], nano carbon fiber [61–

63] and other carbonaceous anodes [64–67] (listed in Supporting Information Table S3). Fig. 6d shows that even after 1000 cycles at the rate of 1 C, the discharge capacity can be stabilized at 297 mAh g^{-1} without fading. In contrast, the sodium-ion devices based on the 3DPG electrode retains 87% of its initial capacity. We tested three batches of 3DGNW anodes and the result is fairly reproducible. From the electrochemical impedance spectroscopy (EIS) data shown in Fig. S19, the obtained charge transfer resistance (R_1) of the 3DGNW anode is ca. 210 Ω, which is much lower than that of 3DGP anode (ca. 320 Ω). The steep liner part in the low frequency region of the 3DGNW electrode also implies its faster ion diffusion process. To gain further insight into the electrode changes upon sodium ion insertion/extraction cycles, the EIS is monitored at various cycles. The fitted sodium charge transfer resistances (R_1) corresponding to the Nyquist plots are shown in Fig. 6e. It should be noted that the R_1 values decrease in the first 500 cycles and then stable in 500–1000 cycles. We propose that electrolyte gradually penetrates onto the surface of GNW and diffuses into the graphene layers after the first 500 cycles, facilitating the electrochemical reaction and leading to the decrease of R_1. The SEM images of 3DGNW electrode after 1000 cycles are shown in Fig. S20. A robust crosslinked network is formed, which is benefited to decrease the resistance and improve the cycle stability of the electrode. Besides, this integrated electrochemical Na storage performance of 3DGNW electrode is superior to previous reported carbonaceous anodes. (see Fig. 6g and comparison in Supporting Information Table S3).

4. Conclusions

In summary, we present a strategy for the assembly of high quality graphene nanowires on 3D graphene foam to form a self-supported and binder-free flexible electrode. When served as anode for Li ion batteries, the 3DGNW anode delivers a high reversible capacity of ca. 545 mAh g^{-1} at 0.1 C rate, and high rate capability of 201 mAh g^{-1} at 20 C. The 3DGNW electrode is also suitable for using as the anode for Na ion batteries, and delivers ultrahigh rate capability of more than 200 mAh g^{-1} at 20 C, and long-term cycling stability of 1000 cycles at 1 C. The outstanding electrochemical performance of this new graphene-based electrode derives from its unique physical and chemical properties, i.e. extensively lateral exposed edges/pores, expansile graphene interlayer distance and relatively low discharge plateau between graphene and graphite. Our results might be a milestone in the development of new types all carbon anodes for next-generation (e.g., Li, Na, K, Ca, and Mg) batteries.

Acknowledgment

The authors would like to acknowledge support from the National Natural Science Foundation of China (No. 51572058, 51307046, 91216123, 51174063, 51502057), the Natural Science Foundation of Heilongjiang Province (E201436), the International Science & Technology Cooperation Program of China (2013DFR10630, 2015DFE52770) and Specialized Research Fund for the Doctoral Program of Higher Education (SRFDP 20132302110031), Natural Science Foundation of Heilongjiang Province of China (Grant No. E2016062), the China Postdoctoral Science Foundation (General Financial Grant No. 2014M561345), the Heilongjiang Postdoctoral Science Foundation (LBH-Z14105), the Scientific Research Foundation for the Returned Overseas Chinese Scholars of the State Education Ministry (No. 20151098), the University Nursing Program for Young Scholars with Creative Talents in Heilongjiang province (No. 2015082), and the Open Project Program of the Key Laboratory for Photonic and Electric Band Gap Materials of the Ministry of Education of Harbin Normal University (No. PEBM201405), postdoctoral scientific research developmental fund of Henlongjiang Province(LBH-Q14144),The Research Foundation for the Returned Overseas Chinese excellent Scholars of Heilongjiang Province (No. 2015424). This work was supported by BSRF Beijing (2016-BEPC-PT-000646).

Appendix A. Supporting information

Supplementary data associated with this article can be found in the online version at doi:10.1016/j.nanoen.2017.04.051.

References

[1] Z.B. Lei, J.T. Zhang, L.L. Zhang, N.A. Kumar, X.S. Zhao, Energy Environ. Sci. 9 (2016) 1891–1930.
[2] X.X. Liu, D.L. Chao, Q. Zhang, H. Liu, H.L. Hu, J.P. Zhao, Y. Li, Y.Z. Huang, J.Y. Lin, Z.X. Shen, Sci. Rep.-Uk 5 (2015).
[3] D.S. Yu, K. Goh, H. Wang, L. Wei, W.C. Jiang, Q. Zhang, L.M. Dai, Y. Chen, Nat. Nanotechnol. 9 (2014) 555–562.
[4] X.X. Liu, D.L. Chao, Y. Li, J. Hao, X.S. Liu, J.P. Zhao, J.Y. Lin, H.J. Fan, Z.X. Shen, Nano Energy 17 (2015) 43–51.
[5] J. Yang, G.Q. Qi, Y. Liu, R.Y. Bao, Z.Y. Liu, W. Yang, B.H. Xie, M.B. Yang, Carbon 100 (2016) 693–702.
[6] L. Wen, F. Li, H.M. Cheng, Adv. Mater. 28 (2016) 4306–4337.
[7] X.X. Liu, J.L. Liu, D. Zhan, J.X. Yan, J. Wang, D.L. Chao, L.F. Lai, M.H. Chen, J.H. Yin, Z.X. Shen, Rsc Adv. 3 (2013) 11601–11606.
[8] D. Chao, P. Liang, Z. Chen, L. Bai, H. Shen, X. Liu, X. Xia, Y. Zhao, S.V. Savilov, J. Lin, Z.X. Shen, ACS Nano 10 (2016) 10211–10219.
[9] D. Chao, C. Zhu, P. Yang, X. Xia, J. Liu, J. Wang, X. Fan, S.V. Savilov, J. Lin, H.J. Fan, Z.X. Shen, Nat. Commun. 7 (2016) 12122.
[10] K.S.N.A.K. Geim, Nat. Mater. 6 (2007) 183–191.
[11] X.J. Alfonso Reina, John Ho, Daniel Nezich, Hyungbin Son, Vladimir Bulovic, Mildred S. Dresselhaus and Jing Kong, Nano Lett., 9, 2009, pp. 30–35.
[12] K.R. Paton, E. Varrla, C. Backes, R.J. Smith, U. Khan, A. O'Neill, C. Boland, M. Lotya, O.M. Istrate, P. King, T. Higgins, S. Barwich, P. May, P. Puczkarski, I. Ahmed, M. Moebius, H. Pettersson, E. Long, J. Coelho, S.E. O'Brien, E.K. McGuire, B.M. Sanchez, G.S. Duesberg, N. McEvoy, T.J. Pennycook, C. Downing, A. Crossley, V. Nicolosi, J.N. Coleman, Nat. Mater. 13 (2014) 624–630.
[13] W.S. Hummers, R.E. Offeman, J. Am. Chem. Soc. 80 (1958) (1339-1339).
[14] D.C. Marcano, D.V. Kosynkin, J.M. Berlin, A. Sinitskii, Z.Z. Sun, A. Slesarev, L.B. Alemany, W. Lu, J.M. Tour, ACS Nano 4 (2010) 4806–4814.
[15] X.X. Liu, D. Zhan, D.L. Chao, B.C. Cao, J.H. Yin, J.P. Zhao, Y. Li, J.Y. Lin, Z.X. Shen, J. Mater. Chem. A 2 (2014) 12166–12170.
[16] M.F. El-Kady, Y. Shao, R.B. Kaner, Nat. Rev. Mater. 1 (2016) 16033.
[17] R. Raccichini, A. Varzi, S. Passerini, B. Scrosati, Nat. Mater. 14 (2015) 271–279.
[18] Y.-X. Wang, S.-L. Chou, H.-K. Liu, S.-X. Dou, Carbon 57 (2013) 202–208.
[19] C.Y. Wang, D. Li, C.O. Too, G.G. Wallace, Chem. Mater. 21 (2009) 2604–2606.
[20] G.X. Wang, X.P. Shen, J. Yao, J. Park, Carbon 47 (2009) 2049–2053.
[21] M. Yan, F. Wang, C. Han, X. Ma, X. Xu, Q. An, L. Xu, C. Niu, Y. Zhao, X. Tian, P. Hu, H. Wu, L. Mai, J. Am. Chem. Soc. 135 (2013) 18176–18182.
[22] Y.J.S. Young-Eun Shin, Seungyoung Park, Jiwon Lee, Kyung-Hee Shin, Sang Hoon Joo, Hyunhyub Ko, Nanoscale Res. Lett. 6 (2014) 7.
[23] Z. Xu, B. Zheng, J. Chen, C. Gao, Chem. Mater. 26 (2014) 6811–6818.
[24] J. Xu, M. Wang, N.P. Wickramaratne, M. Jaroniec, S. Dou, L. Dai, Adv. Mater. 27 (2015) 2042–2048.
[25] E.M. Lotfabad, J. Ding, K. Cui, A. Kohandehghan, W.P. Kalisvaart, M. Hazelton, D. Mitlin, ACS Nano 8 (2014) 7115–7129.
[26] Y. Wen, K. He, Y. Zhu, F. Han, Y. Xu, I. Matsuda, Y. Ishii, J. Cumings, C. Wang, Nat. Commun. 5 (2014) 4033.
[27] H. Hou, C.E. Banks, M. Jing, Y. Zhang, X. Ji, Adv. Mater. 27 (2015) 7861–7866.
[28] B.G. Younan Xia, Yadong Yin, Yu Lu, Adv. Mater. 12 (2000).
[29] I.I. Ahmed, A.K. Gupta, Int. J. Hydrog. Energy 34 (2009) 6253–6264.
[30] P.J.P. Marcus, A. Worsley, Tammy Y. Olson, Juergen Biener, Joe H. Satcher Jr., Theodore F. Baumann, J. Am. Chem. Soc. 132 (2010) 14067–14069.
[31] Y.-L. Ding, P. Kopold, K. Hahn, P.A. van Aken, J. Maier, Y. Yu, Adv. Funct. Mater. 26 (2016) 1112–1119.
[32] J. Annett, G.L. Cross, Nature 535 (2016) 271–275.
[33] Y.N. Chen, K. Fu, S.Z. Zhu, W. Luo, Y.B. Wang, Y.J. Li, E. Hitz, Y.G. Yao, J.Q. Dai, J.Y. Wan, V.A. Danner, T. Li, L.B. Hu, Nano Lett. 16 (2016) 3616–3623.
[34] R. Mukherjee, A.V. Thomas, A. Krishnamurthy, N. Koratkar, ACS Nano 6 (2012) 7867–7878.
[35] E. Yoo, J. Kim, E. Hosono, H. Zhou, T. Kudo, I. Honma, Nano Lett. 8 (2008) 2277–2282.
[36] H. Masunaga, H. Ogawa, T. Takano, S. Sasaki, S. Goto, T. Tanaka, T. Seike, S. Takahashi, K. Takeshita, N. Nariyama, H. Ohashi, T. Ohata, Y. Furukawa, T. Matsushita, Y. Ishizawa, N. Yagi, M. Takata, H. Kitamura, K. Sakurai, K. Tashiro, A. Takahara, Y. Amamiya, K. Horie, M. Takenaka, T. Kanaya, H. Jinnai, H. Okuda, I. Akiba, I. Takahashi, K. Yamamoto, M. Hikosaka, S. Sakurai, Y. Shinohara, A. Okada, Y. Sugihara, Polym. J. 43 (2011) 471–477.
[37] M.Y. Paik, J.K. Bosworth, D.M. Smilges, E.L. Schwartz, X. Andre, C.K. Ober, Macromolecules 43 (2010) 4253–4260.
[38] D. Babonneau, J. Appl. Crystallogr. 43 (2010) 929–936.
[39] W. Wang, X. Chen, Q. Cai, G. Mo, L.S. Jiang, K. Zhang, Z.J. Chen, Z.H. Wu, W. Pan, Eur. Phys. J. B 65 (2008) 57–64.
[40] A.C. Ferrari, J. Robertson, Phys. Rev. B 61 (2000) 14095–14107.
[41] A. Das, S. Pisana, B. Chakraborty, S. Piscanec, S.K. Saha, U.V. Waghmare, K.S. Novoselov, H.R. Krishnamurthy, A.K. Geim, A.C. Ferrari, A.K. Sood, Nat. Nanotechnol. 3 (2008) 210–215.
[42] D. Zhan, L. Sun, Z.H. Ni, L. Liu, X.F. Fan, Y.Y. Wang, T. Yu, Y.M. Lam, W. Huang,

Z.X. Shen, Adv. Funct. Mater. 20 (2010) 3504–3509.
[43] J. Ding, H. Wang, Z. Li, K. Cui, D. Karpuzov, X. Tan, A. Kohandehghan, D. Mitlin, Energy Environ. Sci. 8 (2015) 941–955.
[44] C.-Y. Su, Y. Xu, W. Zhang, J. Zhao, X. Tang, C.-H. Tsai, L.-J. Li, Chem. Mater. 21 (2009) 5674–5680.
[45] D.C. Lin, Y.Y. Liu, Z. Liang, H.W. Lee, J. Sun, H.T. Wang, K. Yan, J. Xie, Y. Cui, Nat. Nanotechnol. 11 (2016) 626.
[46] S.H. Choi, J.-K. Lee, Y.C. Kang, Nano Res. 8 (2015) 1584–1594.
[47] S. Liu, K. Chen, Y. Fu, S. Yu, Z. Bao, Appl. Surf. Sci. 258 (2012) 5299–5303.
[48] S. Li, Y. Luo, W. Lv, W. Yu, S. Wu, P. Hou, Q. Yang, Q. Meng, C. Liu, H.-M. Cheng, Adv. Energy Mater. 1 (2011) 486–490.
[49] F. Liu, S. Song, D. Xue, H. Zhang, Adv. Mater. 24 (2012) 1089–1094.
[50] C.M.H. Xin Zhao, Mayfair C. Kung, Harold H. Kung, ACS Nano 5 (2011) 10.
[51] X.F. Luo, C.H. Yang, Y.Y. Peng, N.W. Pu, M.D. Ger, C.T. Hsieh, J.K. Chang, J. Mater. Chem. A 3 (2015) 10320–10326.
[52] J.T. Xu, M. Wang, N.P. Wickramaratne, M. Jaroniec, S.X. Dou, L.M. Dai, Adv. Mater. 27 (2015) 2042–2048.
[53] X.S. Zhou, X.S. Zhu, X. Liu, Y. Xu, Y.X. Liu, Z.H. Dai, J.C. Bao, J. Phys. Chem. C 118 (2014) 22426–22431.
[54] Y. Yan, Y.X. Yin, Y.G. Guo, L.J. Wan, Adv. Energy Mater. 4 (2014).
[55] J. Zhang, Z. Zhang, X.X. Zhao, RSC Adv. 5 (2015) 104822–104828.
[56] B. Jache, P. Adelhelm, Angew. Chem. Int. Ed. 53 (2014) 10169–10173.
[57] Z.Q. Zhu, F.Y. Cheng, Z. Hu, Z.Q. Niu, J. Chen, J. Power Sources 293 (2015) 626–634.
[58] P.X. Han, X.Q. Han, J.H. Yao, Z.H. Liu, X.Y. Cao, G.L. Cui, Electrochem. Commun. 61 (2015) 84–88.
[59] S. Komaba, W. Murata, T. Ishikawa, N. Yabuuchi, T. Ozeki, T. Nakayama, A. Ogata, K. Gotoh, K. Fujiwara, Adv. Funct. Mater. 21 (2011) 3859–3867.
[60] A. Fukunaga, T. Nohira, R. Hagiwara, K. Numata, E. Itani, S. Sakai, K. Nitta, S. Inazawa, J. Power Sources 246 (2014) 387–391.
[61] W. Luo, J. Schardt, C. Bommier, B. Wang, J. Razink, J. Simonsen, X. Ji, J. Mater. Chem. A 1 (2013) 10662.
[62] Y. Liu, F. Fan, J. Wang, H. Chen, K.L. Jungjohann, Y. Xu, Y. Zhu, D. Bigio, T. Zhu, C. Wang, Nano Lett. 14 (2014) 3445–3452.
[63] T. Chen, Y. Liu, L. Pan, T. Lu, Y. Yao, Z. Sun, D.H.C. Chua, Q. Chen, J. Mater. Chem. A 2 (2014) 4117.
[64] K. Tang, L. Fu, R.J. White, L. Yu, M.-M. Titirici, M. Antonietti, J. Maier, Adv. Energy Mater. 2 (2012) 873–877.
[65] H.W. Jia Ding, Zhi Li, Alireza Kohandehghan, Kai Cui, Zhanwei Xu, Beniamin Zahiri, Xuehai Tan, Elmira Memarzadeh Lotfabad, Brian C. Olsen, David Mitlin, ACS Nano 7 (2013) 11004–11015.
[66] X. Zhou, Y.-G. Guo, Chemelectrochem 1 (2014) 83–86.
[67] S. Wenzel, T. Hara, J. Janek, P. Adelhelm, Energy Environ. Sci. 4 (2011) 3342.

Dr. Xiaoxu Liu received the M.S in Physics from Harbin Normal University (Harbin, China, 2007), and the Ph.D in College of Materials Science and Engineering, from Harbin University of Science and Technology (China, 2012). He was research fellow in School of Physical and Mathematical Sciences at Nanyang Technological University. He has been an associate Professor in Heilongjiang University of Science and Technology. His current research interests mainly focus on design, fabrication and application of graphene based composite.

Dongliang Chao, started his Ph.D. study at Nanyang Technological University (NTU) under Prof. Ze Xiang Shen in 2013, and he joined Prof. Bruce Dunn's group in 2016 at University of California, Los Angeles as exchange student. Currently, he is working as Research-Associate under Prof. Hong Jin Fan at NTU. His research focuses on graphene based hybrid electrodes, and pseudocapacitive behaviors in batteries electrode for rechargeable energy storage and conversion. He has published ~20 first/co-first-author papers in his Ph.D. studies, e.g. Nat. Commun., Adv. Mater., Nano Lett., ACS Nano, Nano Today, etc. with 10 ESI highly cited papers.

Dapeng Su is currently working at ZTE Corporation, China. He received his masters degree in School of Chemical Engineering and Technology, Harbin Institute of Technology. His focus is on the design, fabrication and characterization of 3D Graphene-based materials for energy storage.

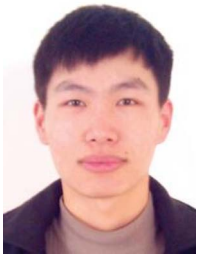

Shikun Liu received his Master's degree in QiLu University of Technology. He is currently pursuing his Ph.D. degree at School of Chemistry and Chemical Engineering, Harbin Institute of Technology under supervision of Prof. Jiupeng Zhao. His research interests mainly focus on the design and synthesis of nanomaterials for energy conversion and storage devices.

Liang Chen received his B.S. degrees in Heilongjiang University. He is currently a M.S. candidate under supervision of Prof. Jiupeng Zhao at School of Chemical Engineering, Harbin Institute of Technology. His research interests mainly focus on design, fabrication and characterization of graphene-based materials for energy storage.

Caixia Chi received her MSc degrees in Changchun University of Science and Technology. She is currently a Ph.D. candidate under supervision of Prof. Jiupeng Zhao at School of Chemistry and Chemical Engineering, Harbin Institute of Technology. Her research interests mainly focus on design, fabrication and characterization of Ge-based materials for energy storage.

Prof. Jianyi Lin is currently a project consultant at Institute of Chemical and Engineering Sciences (ICES), A*STAR, Singapore, and an Adjunct Professor in the Department of Physics, National University of Singapore (NUS). He graduated from Xiamen University, China and received PhD in Chemistry from Stanford University in 1991. His research and expertise areas lie in surface science, heterogeneous catalysis and nano-materials, which include hydrogen production and storage, PEM fuel cell, supercapacitor and Li-ion battery studies.

Dr. Ze Xiang Shen is a professor in the School of Physical and Mathematical Sciences, and the School of Materials Science and Engineering, Nanyang Technological University. He is the Program Chair of the Interdisciplinary Graduate School. He concurrently holds the position of Co-Director, Center for Disruptive Photonics Technologies. His research areas include carbon related materials, especially graphene. His work involves spectroscopic and theoretical study of few-layer graphene and folded graphene, graphene based composites for energy harvesting and nanoelectronics, as well as fundamentals on electronic structures, doping, and intercalation. He also works on developing near-field Raman spectroscopy/imaging techniques and the study of plasmonics structures.

Dr. Jiupeng Zhao received her Ph.D. degree from Harbin Institute of Technology (HIT) in 2000. She has been a Professor in School of Chemical Engineering and Technology at HIT since 2007. Her research is focusing on the design and fabrication of nanostructured materials for energy storage applications and electrical devices.

Liqiang Mai is Chair Professor of Materials Science and Engineering at Wuhan University of Technology (WUT). He received his Ph.D. from WUT in 2004. He carried out his postdoctoral research in the laboratory of Prof. Zhonglin Wang at Georgia Institute of Technology in 2006–2007 and worked as advanced research scholar in the laboratory of Prof. Charles M. Lieber at Harvard University in 2008–2011. He worked as advanced research scholar in the laboratory of Prof. Peidong Yang at University of California, Berkeley in 2017. His current research interests focus on nanowire materials and devices for energy storage. He received the National Natural Science Fund for Distinguished Young Scholars, the China Youth Science and Technology Award and so forth.

Yao Li has been a Professor of Materials Science in Harbin Institute of Technology (HIT) since 2005 and leads the laboratory of Functional Composite Materials in Center for Composite Materials. His research interests include fabrication and engineering nanostructured inorganic materials and polymers with well-defined microstructure and multiple length scales, and their applications for energy storage, and electrochromism. He is the author or co-author of over 120 papers, 62 patents, and 3 books in the fields of materials science and processing. He was selected as “The Yangtze River scholar Professor” by Ministry of Education, New Century Excellent Talents program” and “Distinguished Young Scholars for Heilongjiang Province” and “Youth leader in Science and Technology Innovation” by Ministry of Science and Technology. He was awarded “Science and Technology Award for the Youth of China”, “National Award of the outstanding Scientific and Technological Workers” and “the first Prize of Natural Science of Heilongjiang Province”. He is the council member of Chinese Materials Research Society and Functional Materials Society of China.